Nanoarchitectonics
http://ojs.wiserpub.com/index.php/NAT/

UNIVERSAL WISER PUBLISHER

Research Article

Porous Carbons Derived from Ginkgo Shell Used for High-Performance Supercapacitors

Yu Wang, Ying Zhu, Hailiang Chu, Shujun Qiu*, Yongjin Zou, Cuili Xiang, Huanzhi Zhang, Kexiang Zhang, Erhu Yan, Bin Li, Dan Cai, Xiangcheng Lin, Hongliang Peng, Xin Wen, Fen Xu, Lixian Sun*

Guangxi Key Laboratory of Information Materials, Guangxi Collaborative Innovation Center of Structure and Property for New Energy and Materials and School of Materials Science and Engineering, Guilin University of Electronic Technology, Guilin, 541004, China
E-mail: qiushujun@guet.edu.cn (S. Qiu), sunlx@guet.edu.cn (L. Sun)

Received: 6 July 2020; **Revised:** 1 August 2020; **Accepted:** 28 August 2020

Abstract: As a renewable biomass and a low-cost crude carbon source, the ginkgo shell is explored for preparing high-value porous carbon via carbonization and the following KOH activation. Structure characterization shows that GSPC has microporous and mesoporous structure with specific surface area (SSA) of up to 1941 $m^2 g^{-1}$, which exhibits superior capacitive properties. In a three-electrode system by using 6 M KOH as electrolyte, GSPC-700-1:2 could deliver a high specific capacitance of 345 F g^{-1} at 0.5 A g^{-1}. Even at a high current density of 20 A g^{-1}, the specific capacitance of as high as 280 F g^{-1} can be still maintained. Furthermore, a symmetric supercapacitor device (SCD) is fabricated by GSPC-700-1:2, which exhibits a capacitance retention rate of 83% at 5 A g^{-1} after 10000 charging/discharging cycles. A power density of 301 W kg^{-1} is achieved at an energy density of 13 W h kg^{-1}. The superior electrochemical performance demonstrates that ginkgo shell can function as a new biomass material for the production of porous carbon materials that are used in high-performance supercapacitors and other energy storage devices.

***Keywords*:** supercapacitor, ginkgo shell, porous carbons, KOH activation

1. Introduction

Energy is not only the lifeblood of a country's rapid economic development, but also the material basis for human survival [1]. At present, with the increasing consumption of fossil energy and the accompanying harsh environmental pollution, people around the world are paying much attention to the development of environmentally friendly and sustainable clean energy technologies [2]. In recent years, China has also continuously increased its investment in energy-saving, environmentally friendly and renewable clean energy technologies [3]. Through the continuous exploration of scientists, a large number of renewable clean energy has been rapidly developed [4]. Technologies such as wind power generation, solar cells and geothermal heating have been successfully applied to the real life. However, due to development costs and technical level limitations, they have not been fully popularized.

Therefore, research and development of electric devices for sustainable energy conversion and storage is an important way for efficient use of the aforementioned clean energy technologies. As a kind of electric storage device, supercapacitor has attracted widespread attention due to its high power density and long cycle life in recent years [5]. It

DOI: https://doi.org/10.37256/nat.212021533

fills the gap between traditional electrostatic containers (high power density, low energy density) and chemical batteries (high energy density, low power density) [6] and then has a wide range of applications in the field of short-term high-power output such as high-energy vehicles motor start-up [7]. Recently, supercapacitors have been rapidly developed in many other fields due to their outstanding cycle stability and environmental protection. The supercapacitor is a new energy storage device between conventional capacitor and secondary battery [8]. Compared with conventional capacitors, it has higher specific capacitance and energy density, wider operating temperature range and longer cycle life. While compared to lithium secondary batteries [9], with higher specific power, it can release a large current in a very short time. Moreover, it has the advantages of faster charging speed, higher charging efficiency, and longer cycle life [10].

Supercapacitors can be divided into electric double layer capacitors (EDLC) and pseudocapacitors based on the different charge storage mechanisms. The storage mechanism of EDLC is to form an electric double layer at the interface where the carbon electrode material contacts the electrolyte to generate electric capacity; while the capacitance of pseudocapacitors is derived from the reversible redox reaction of the electrode material [11]. No matter what kind of supercapacitors, porous carbon materials are commonly used electrode materials due to the advantages of large specific surface area, adjustable pore structure, high conductivity, good chemical stability, etc. They are brilliant in the field of energy storage, especially in the application of EDLC electrode materials [12]. As abundant raw materials for preparing carbon materials, biomass mainly includes raw biomass (shells, stems, leaves, etc.) and some biomass derivatives (cellulose, hemicellulose, lignin, protein, melanin, amino acids, sugars, etc.) [13-15]. Biomass-derived functional carbon materials are valued in the field of energy storage and most biomass precursors are rich of heteroatoms such as nitrogen and oxygen [16].

The preparation of biomass-derived carbon has a significant effect on its porous structure (macropores, mesopores and micropores), surface functional groups and graphitization. In order to control the structure and properties of carbon materials, new synthesizing methods such as hydrothermal method, molten salt carbonization method and template method were proposed [17]. However, these methods for synthesizing carbon materials are expensive and time-consuming.

Ginkgo biloba is a precious tree species. So far, ginkgo shells have been used as a by-product of ginkgo processing only for feed or discarded, resulting in a great waste of resources. Therefore, the synthesis of porous carbon materials from ginkgo shells is of great significance for the application of high-performance supercapacitors. In this study, we employ a low-cost and simple method to prepare ginkgo shell-derived porous carbon (GSPC). This method can produce GSPC on a large scale and has great commercial application prospects [18]. The ginkgo shells are used as the carbonization precursor and then react with KOH as the activator to produce porous carbon materials. The obtained GSPC exhibits a higher specific surface area (SSA) of 1942 m^2 g^{-1}. In a three-electrode system using an alkaline solution (6 M KOH) as an electrolyte, a high capacitance of 345 F g^{-1} at 0.5 A g^{-1} is achieved. Moreover, a symmetric supercapacitor device (SCD) is fabricated by GSPC, which shows superior electrochemical properties.

2. Experimental

2.1 *Reagents and materials*

Ginkgo shells were collected from Huajiang campus of Guilin University of Electronic Technology on Oct. 2018. KOH was purchased from Xilong Chemical Co., Ltd. All the chemical reagents in this work were analytical grade and used without further purification.

2.2 *Preparation of porous carbons from ginkgo shell*

For the typical synthesis of the porous carbon materials, ginkgo shells were first washed with deionized water to completely remove adhered dirt, and then dried at 100°C for 24 h to remove the moisture contents. The dried ginkgo shells were ground and sieved to the particles sizes of 2 ~ 8 mm and then pre-carbonized at 400°C for 2 h under a protective atmosphere of nitrogen at a heating rate of 5°C min^{-1}. The pre-carbonized samples were then mixed with KOH in a mass ratio of 1:2 and dissolved in deionized water under magnetic stirring for 1 h, then dried at 100°C overnight. Next, the

resultant samples were carbonized at 700°C for 2 h under nitrogen atmosphere with a heating rate of 5°C min^{-1}. After being naturally cooled down to room temperature, the final samples were washed with 1 M HCl solution and deionized water until pH of the solution after washing reached to be about 7, and then dried at 60°C overnight, which was named as GSPC-700-1:2. For comparison, we also prepared a series of control samples by changing the amount of KOH (the mass ratio of pre-carbonized sample to KOH was set as 1:0, 1:1 and 1:3) while other reaction conditions are same as the above typical preparation. These samples obtained at different ratios are recorded as GSPC-700-1:0, GSPC-700-1:1, and GSPC-700-1:3, respectively.

2.3 *Morphological and microstructural characterization*

Hitachi S-4700 scanning electron microscope (SEM) and JEOL-2100 transmission electron microscope (TEM) were used to characterize the morphology and microstructure of GSPC samples. X-ray powder diffraction (XRD) patterns were recorded by a Bruker D8 advance diffractometer with Cu-Kα radiation. The nitrogen adsorption-desorption isotherms of the as-prepared samples were measured on a Quadra chrome adsorption instrument at 77 K, and the total specific surface area (SSA) of the samples was calculated by the Brunauer-Emmett-Teller (BET) method. The pore size distribution was obtained by using BJH method. X-ray photoelectron spectroscopy (XPS) was carried out on a VG ESCALAB MK II X-ray photoelectron spectrometer (VG Scientific). An HR700-type laser Raman spectrometer was used to test the samples at an excitation wavelength of 458 nm.

2.4. *Electrochemical performance*

To measure the electrochemical properties of GSPC samples, an electrode for supercapacitor was first fabricated. GSPC, acetylene black and poly (tetrafluoroethylene) were mixed in a mass ratio of 80:10:10, and the mixture was pressed at 8 MPa on nickel foam ($2 * 2$ cm^2) to form a working electrode with a mass loading of about 1.5 mg cm^{-2}. Electrochemical measurements were sequentially performed in a KOH solution using a CHI660E electrochemical workstation. Platinum sheet and Hg/HgO were used as the counter electrode and the reference electrode, respectively. Cyclic voltammetry (CV) analysis was performed in alkaline solution (6 M KOH) over a potential range of -1 ~ 0 V and a galvanostatic charge-discharge (GCD) test was conducted within voltage range of -1 ~ 0 V. The specific gravimetric capacitance was calculated by the following Formula:

$$C = \frac{I\Delta t}{m\Delta V} \tag{1}$$

where m (g) is the mass of active substance, ΔV (V) is the voltage change (not including the IR drop during the discharge process), I (A) is the current density, and Δt (s) is the discharge time.

In the two-electrode system, the working voltage range of CV test and GCD test was 0 ~ 1.2 V. The specific capacitance of SCD was calculated according to the Formula (1) based on the total mass of electrodes. The energy density (E_t) and the power density (P_t) of SCD were calculated using the following equations:

$$E_t = \frac{Ct(\Delta V)^2}{2 \times 3.6} \tag{2}$$

$$P_t = \frac{E_t}{t} \times 3600 \tag{3}$$

3. Results and discussion

The fabrication process of ginkgo shell-derived porous carbon (GSPC) is clearly shown in Figure (1), which involves a pre-carbonization process and the following activation process by using KOH under nitrogen atmosphere.

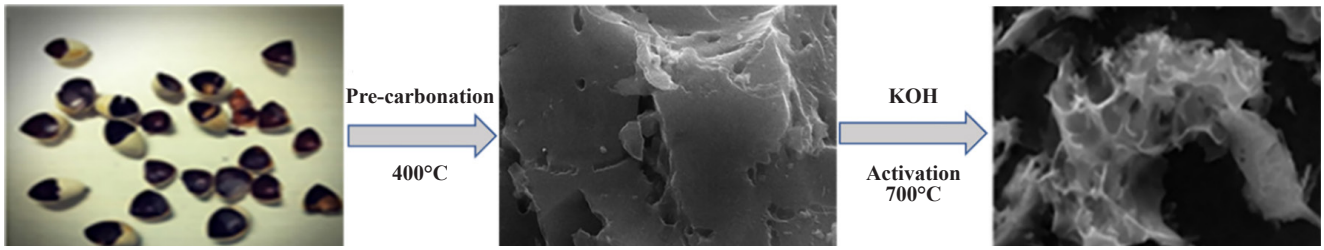

Figure 1. Diagram of preparation of GSPC samples

The surface morphology of GSPC samples is characterized by scanning electron microscopy (SEM). Figure 2 (a) shows that the pre-carbonized sample is in the form of porous networks and has a relatively smooth surface. The samples without KOH activation are characterized by a layered structure and no obvious pores are observed. The morphology of the samples after being activated by KOH is shown in Figure 2 (b, c and d). It can be clearly seen that their structure has changed significantly. As shown in Figure 2 (b), after GSPC sample was etched by KOH, the sample surface was no longer smooth. With the increase of KOH content, as shown in Figure 2 (c), GSPC sample has formed a porous network structure, and the structure is relatively uniform. This special structure can help improve ion transfer by providing pathways for electrolyte ion transmission and penetration. However, as the amount of KOH continues to increase, the pores on the surface of GSPC samples become larger and larger, which results in the collapse of the porous network structure and thus affects the electrochemical performance. Moreover, compared with GSPC-700-1:0 in Figure 2 (e), a rough surface is also clearly observed from TEM image of GSPC-700-1:2 (Figure 2 (f)). Rough surfaces can facilitate the bulk charge storage, thus improving electron transport capability. The uniform distribution of carbon and oxygen elements in GSPC-700-1:2 is observed in Figure 2 (g and h).

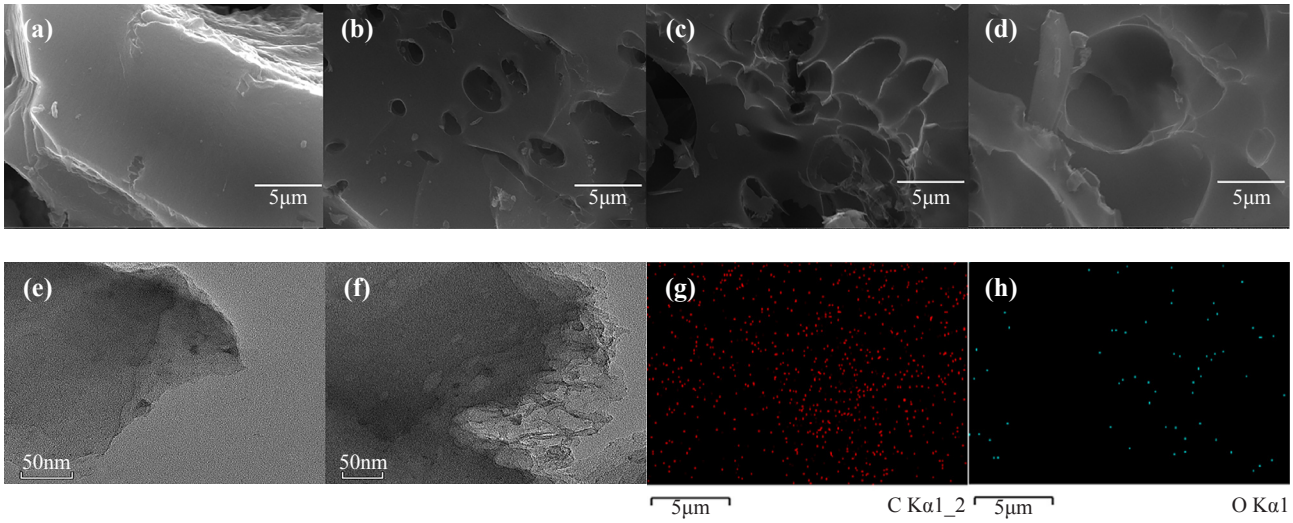

Figure 2. SEM images of (a) GSPC-700-1:0, (b) GSPC-700-1:1, (c) GSPC-700-1:2 and (d) GSPC-700-1:3. TEM images of (e) GSPC-700-1:0 and (f) GSPC-700-1:2. (g and h) EDS mappings of GSPC-700-1:2

The nitrogen adsorption-desorption isotherm is used to measure the specific surface area and pore size of GSPC samples. As shown in Figure 3 (a), all GSPCs clearly show type I adsorption-desorption isotherms. At lower relative pressures (P/P_0), the N_2 adsorption isotherm increased, indicating that GSPC contains micropores. Figure 3 (b) shows the pore size distribution of GSPC sample. GSPC-700-1:1, GSPC-700-1:2 and GSPC-700-1:3 are mainly composed of micropores and mesopores. Especially for GSPC-700-1:2, it contains a large number of micropores and a small amount of mesopores, which thus leads to an increase of SSA and provides more active sites for charge accumulation,

thereby increasing the capacitance of the electric double layer [19]. The specific properties of GSPC materials are summarized in Table 1. SSAs of GSPC-700-1:1, GSPC-700-1:2 and GSPC-700-1:3 are identified as 1380, 1941 and 1471 $m^2 g^{-1}$, respectively. These data indicate that as the amount of KOH increases, SSA increases, which indicates that the corrosion of the pre-carbonized samples becomes more severe as the KOH content increases. However, for GSPC-700-1:3, excessive KOH will cause structural damage and result in a smaller SSA. Rupture of micropores in the sample may lead to the formation of small mesopores. This hierarchical porous structure with the coexistence of mesopores and micropores is necessary for a carbonaceous material used as electrodes in supercapacitors. Moreover, mesopores can provide a wider transport path than micropores, thereby promoting better adsorption [20].

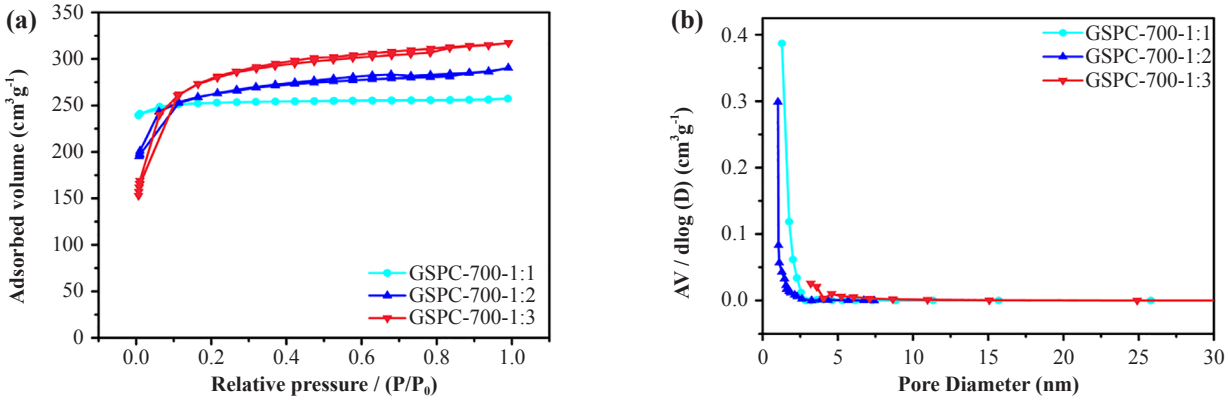

Figure 3. (a) Nitrogen absorption/desorption isotherms and (b) corresponding pore size distribution plots of GSPC samples

Table 1. Textural characteristics of GSPC samples based on nitrogen sorption isotherms and Raman spectra

Sample	BET SSA ($m^2 g^{-1}$)				Micropore volume ($cm^3 g^{-1}$)	I_D/I_G [b]
	Total	Micro	Meso	Ratio[a]		
GSPC-700-1:1	1380	971	409	2.37	0.340	0.86
GSPC-700-1:2	1941	1138	803	1.42	0.318	0.84
GSPC-700-1:3	1471	1038	433	2.40	0.305	0.85

a) The ratio of micropore to mesopore on SSA.
b) The intensity ratio of D band to G band.

X-ray diffraction pattern of GSPC samples is shown in Figure 4 (a). All GSPC samples show a broad peak at 2θ = 24.8° and a weak peak at 2θ = 42.9°, corresponding to (002) and (110) planes of graphite structure. The observed diffraction pattern indicates that the prepared porous carbon mainly contains a large amount of amorphous carbon [21]. As shown in Figure 4 (b), there are two characteristic absorption peaks are displayed at 1368 cm^{-1} (D band) and 1576 cm^{-1} (G band) in Raman spectra of the as-prepared samples. The D-band peak is a characteristic absorption peak of amorphous carbon and the G-band peak is related to the distribution of sp^2 hybridized carbon atoms in the graphite carbon phase [22]. The intensity ratio of D to G peaks (I_D/I_G) is commonly used to measure the degree of graphitization and the degree of disorder of carbon materials. I_D/I_G values for GSPC-700-1:0, GSPC-700-1:1, GSPC-700-1:2 and GSPC-700-1:3 are 0.85, 0.86, 0.84 and 0.85, respectively. This result shows that the C-atomic lattice defects of four samples are very close [23].

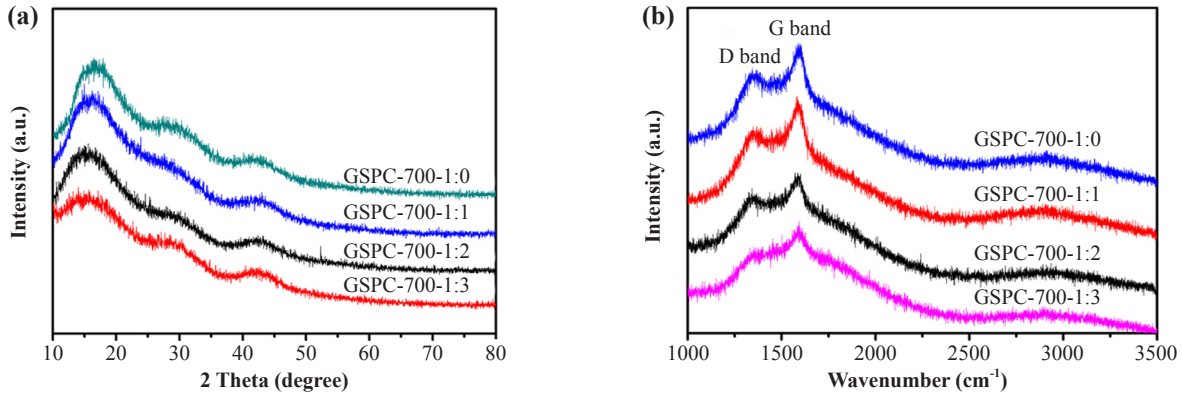

Figure 4. (a) XRD patterns and (b) Raman spectra of GSPC samples

The elemental chemical state on the surface of GSPC samples is measured by using X-ray photoelectron spectroscopy (XPS). From the survey spectra shown in Figure 5 (a), the characteristics peaks of C 1s and O 1s at about 290 and 537 eV are observed, indicating these as-prepared samples contain carbon and oxygen elements. Based on XPS results, the content of carbon and oxygen in GSPC-700-1:2 is 84.49 at.% and 15.51 at.%, respectively. Figures 5 (b and c) show the high-resolution spectra of C 1s and O 1s, where C 1s peak appears at 284.6 eV (C = C), 287.8 eV (C = O) and 285.5 eV (C-C) and O 1s peak appears at 534.2 eV (-O-), 533.1 eV (C-O-C) and 531.9 eV. The peak at 531.9 eV for O 1s is attributed to C-OH probably from alcohols, phenols, aliphatic ethers or other hydroxyl-containing compounds. These functional groups can improve the wettability of the as-prepared samples, thereby increasing the surface activity of GSPC samples [24].

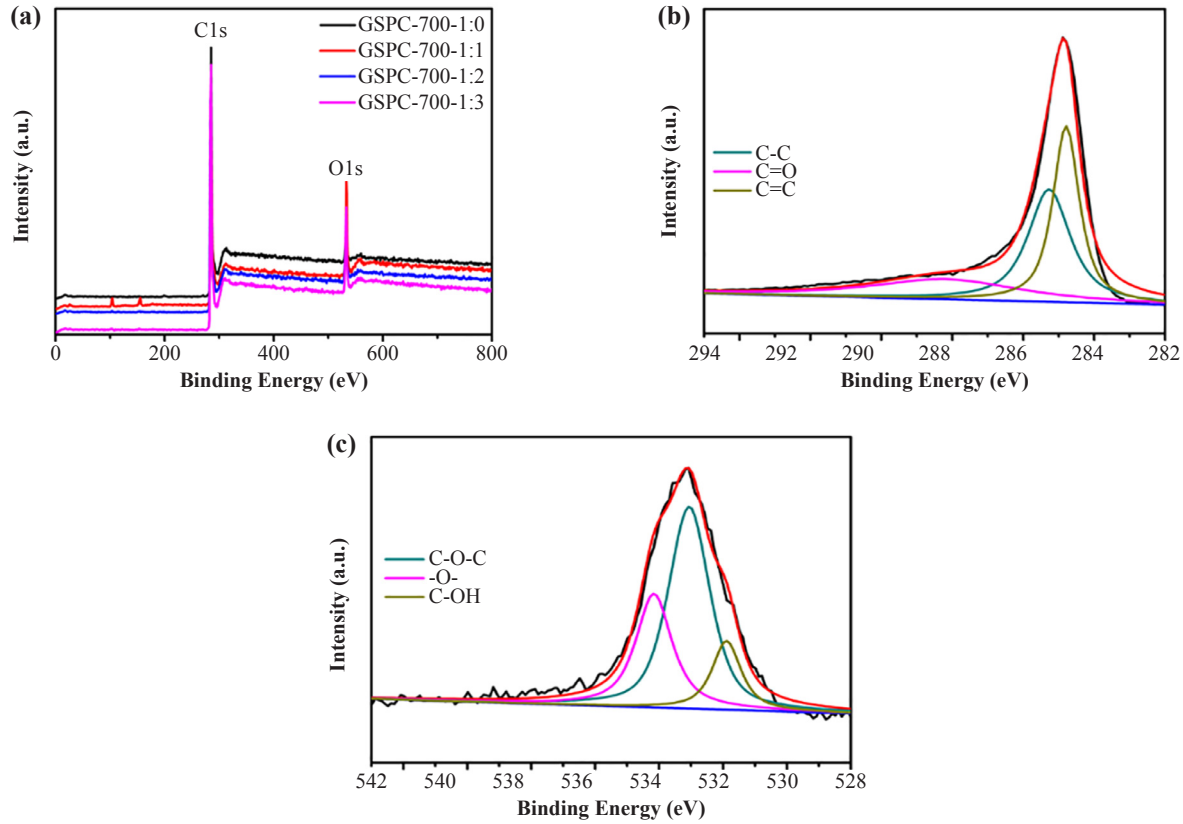

Figure 5. XPS results of (a) survey spectra, (b) C 1s and (c) O 1s of GSPC-700-1:2

In this study, the electrochemical performance of GSPC samples is characterized in a three-electrode system. CV curve of GSPC samples in Figure 6 (a) is measured at a scan rate of 20 mV s^{-1}.-The deviation from the rectangular shape is resulting from the resistance of electrolyte ions diffusion in the micropores. In addition, when the loop is completed, ion diffusion is delayed, resulting in a delay in current response [25-27]. This resultant dispersion capacitance effect also produces a CV curve that deviates from the rectangular shape. However, a comparison of these samples indicates that GSPC-700-1:2 shows a largest rectangular area, indicating the highest specific capacitance. Figure 6 (b) shows the galvanostatic charge and discharge (GCD) curves for GSPC samples at a current density of 1 A g^{-1}. Note that, GCD curves form an approximately symmetrical triangle [28-30] with a transition zone observed between -1 and -0.4 V, which coincides with the location of the protrusions in CV curves. The highest specific capacitance of 345 F g^{-1} is achieved for GSPC-700-1:2 among these four samples. Figure 6 (c) shows the rate capability of GSPC samples conducted at the different current densities of 0.5 ~ 10 A g^{-1}. As the current density increases, the specific capacitance of GSPC samples decreases because the diffusion resistance of the charge in the pores is increased at high current density [31]. Clearly, GSPC-700-1:2 delivers an outstanding rate performance. For example, at a current density of 0.5 A g^{-1}, GSPC-700-1:0, GSPC-700-1:1, GSPC-700-1:2 and GSPC-700-1:3 have a specific capacitance of 152 F g^{-1}, 284 F g^{-1}, 345 F g^{-1}, and 300 F g^{-1}. When the current density is increased to 10 A g^{-1}, the specific capacitance for each sample is decreased to 110 F g^{-1}, 200 F g^{-1}, 280 F g^{-1}, and 220 F g^{-1}, respectively. CV curves of GSPC-700-1:2 measured over a scan rate range of 5 ~ 100 mV s^{-1} in Figure 6 (d) gradually deforms as the scanning rate increases, which indicates that the stored charge is attributed to the two-layer formation mechanism. At high scanning rate of 100 mV s^{-1}, CV curve of GSPC-700-1:2 is almost rectangular, again indicating that it has superior rate performance. Figure 6 (e) shows GCD curves of GSPC-700-1:2 at a current density between 0.5 and 10 A g^{-1}. Almost all curves form an isosceles triangle, indicating a superior electrochemical reversibility. Figure 6 (f) gives the cycling stability at a current density of 20 A g^{-1}. It can be seen that after 10,000 cycles, the specific capacitance retention is as high as 93%. These results indicate that GSPC-700-1:2 exhibits better electrochemical performance, which is superior to other biomass-derived carbon materials used for supercapacitor electrodes (Table 2). In addition, the electrochemical impedance spectroscopy (EIS) in the frequency range of 100 kHz to 0.01 Hz was performed (Figure 6 (g)). Generally, there are two parts in the Nyquist plot [32-34]. One is a semicircular loop in the high-frequency region and the other is a linear component in the low-frequency region [35-37]. Obviously, GSPC-700-1:2 has a higher slope, which represents a lower diffusion resistance [38-40], indicating its better capacitance characteristic. From the enlarged plots in the high frequency region shown in Figure 6(h), GSPC-700-1:2 exhibits the largest semicircle, perhaps because it has a large number of micropores and superior conductivity [41-44]. Moreover, the real-axis intercept corresponds to the internal resistance of the electrochemical system. Among these four samples, GSPC-700-1:2 delivers a minimum internal resistance (0.31 Ω), indicating its higher electrical conductivity.

Table 2. Comparison of electrochemical performance of different biomass derived carbon materials in 6 M KOH using 3-electrode system

Precursor	Specific capacitance		Reference
Broad bean shell	202 F g^{-1}@0.5 A^{g}-1	171 F g^{-1}@10 A g^{-1}	[39]
Tobacco rods	286.6 F g^{-1}@0.5 A g^{-1}	246 F g^{-1}@10 A g^{-1}	[40]
Onion	179 F g^{-1}@1 A g^{-1}	156 F g^{-1}@10 A g^{-1}	[41]
Willow catkin	298 F g^{-1}@0.5 A g^{-1}	270 F g^{-1}@10 A g^{-1}	[42]
Silkworm	306 F g^{-1}@1 A g^{-1}	260 F g^{-1}@10 A g^{-1}	[43]
EWC-2	335 F g^{-1}@0.5 A g^{-1}	270 F g^{-1}@10 A g^{-1}	[44]
Ginkgo shell	345 F g^{-1}@0.5 A g^{-1}	280 F g^{-1}@10 A g^{-1}	This work

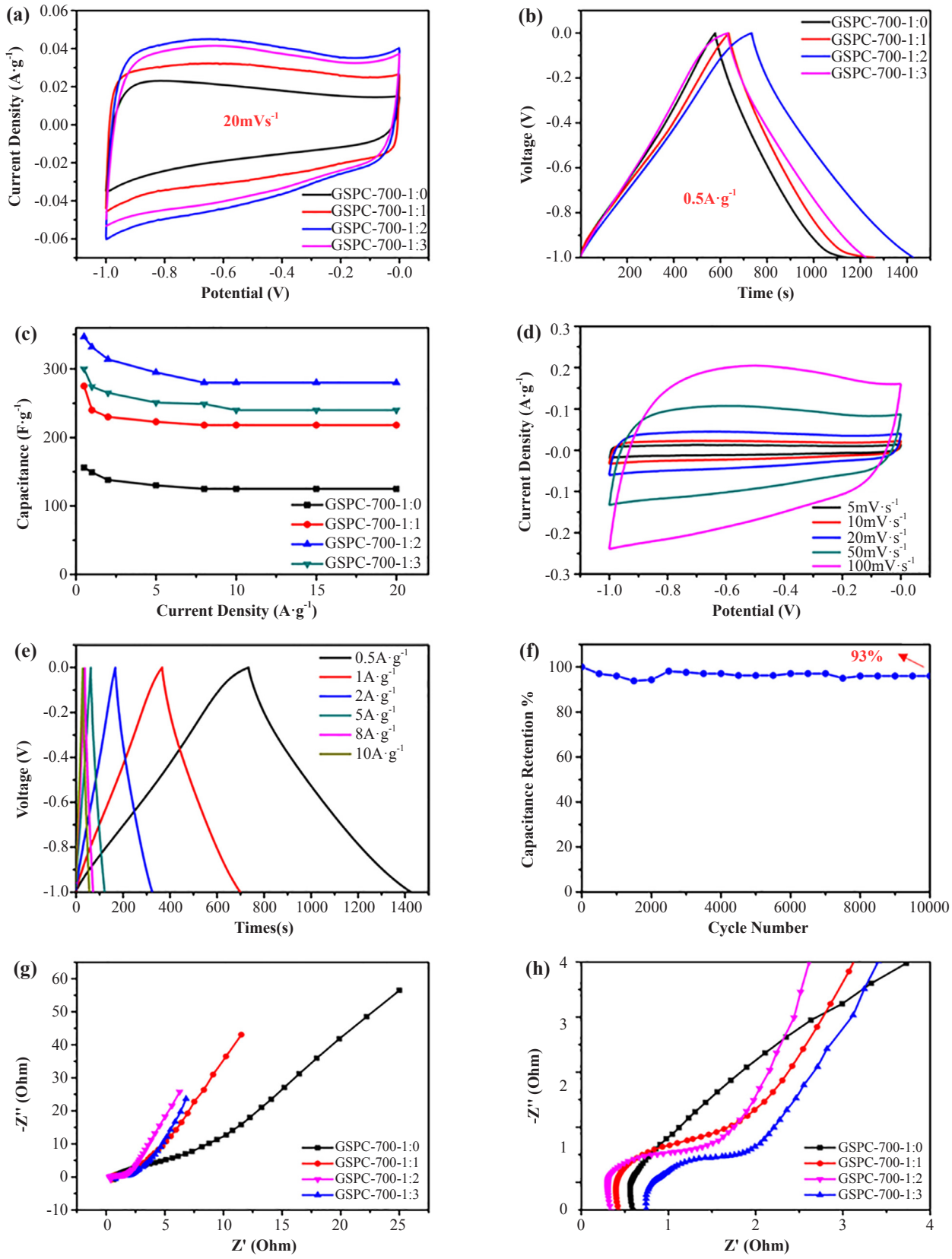

Figure 6. Electrochemical performance of GSPC samples measured in a three-electrode system in 6 M KOH electrolyte: (a) CV curves; (b) GCD curves; (c) Specific capacitances at different current densities. For GSPC-700-1:2, (d) GCD curves at different current densities; (e) CV curves at different scan rates and (f) Cycling stability at a current density of 20 A g^{-1}. (g) Nyquist plots of the samples and (h) The corresponding local enlarged plots at a high-frequency region

The aforementioned performance comparison shows that GSPC-700-1:2 exhibits the best electrochemical performance among four samples. Therefore, a symmetric supercapacitor device (SCD) consisting of two electrodes with the same size is fabricated from GSPC-700-1:2 and the electrochemical performance in 6 M KOH is further characterized. Figure 7 (a) shows CV curve of SCD within different voltage ranges at a scan rate of 100 mV s^{-1}. It can be seen that when the voltage is extended to 1.4 V, an obvious polarization appears in CV curve. Figure 7 (b) shows GCD curve for SCD at different current densities. When the current density is increased from 0.5 to 10 A g^{-1}, the specific capacitance of SCD is decreased from 65 to 42 F g^{-1}. Moreover, the capacitance retention rate is 83% at 5 A g^{-1} after 10,000 cycles in Figure 7 (c), indicating a satisfactory cycling performance. The capacitance decay is probably due to the deactivation of oxygen-containing functional groups on the surface of the activated carbon material [45-47]. Ragone plot of SCD is shown in Figure 7 (d). Note that, a power density of 301 W kg^{-1} is achieved at an energy density of 13 W h kg^{-1}, which is better than that of most reported biomass-derived carbon materials.

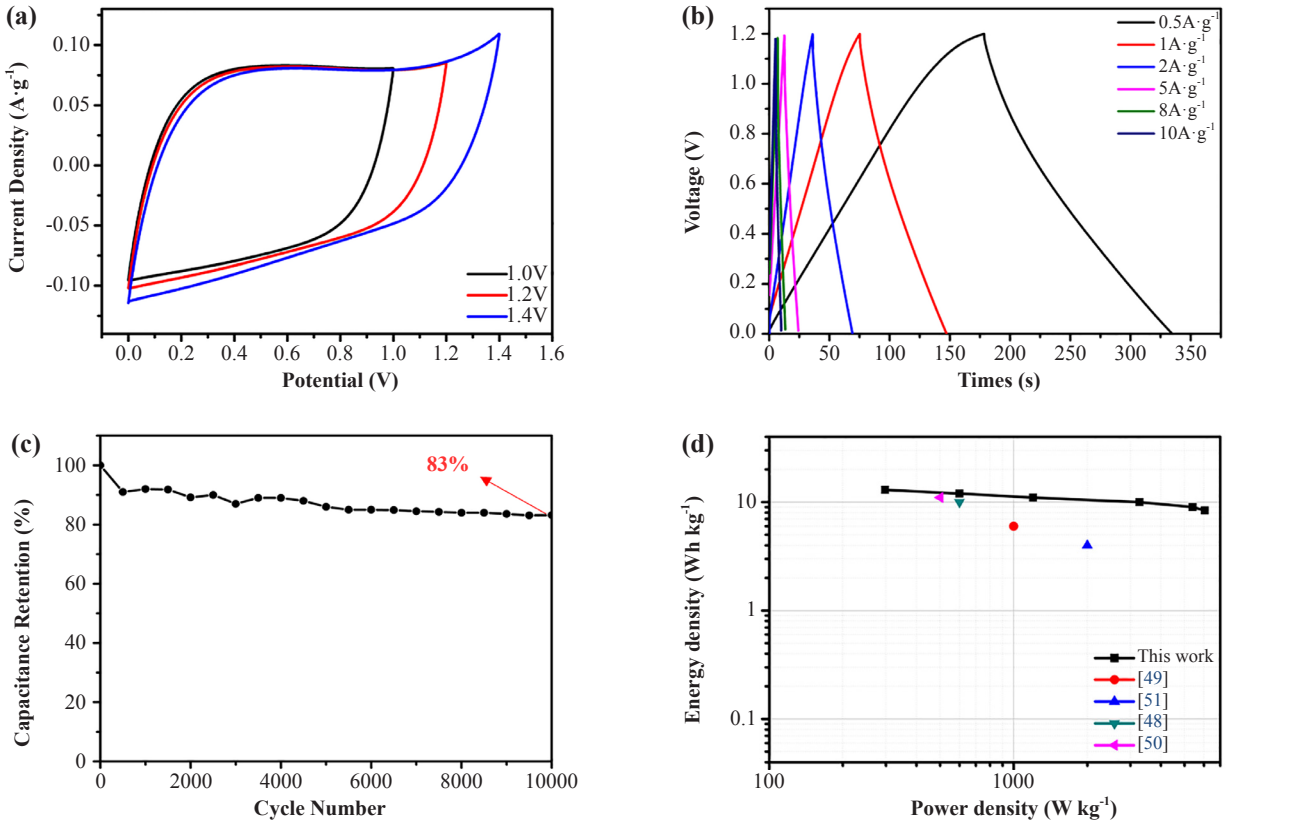

Figure 7. Electrochemical performance of SCD fabricated from GSPC-700-1:2 measured in a two-electrode system using 6 M KOH electrolyte: (a) CV curves at a scan rate of 100 mV s^{-1}; (b) GCD curves at various current densities; (c) Cycling stability at a current density of 5 A g^{-1} and (d) Ragone plots

4. Conclusions

In conclusion, we have successfully produced high-quality porous carbon materials by carbonization and following KOH activation of environmentally friendly renewable ginkgo shells. The synthesis method is simple, inexpensive and easily scalable. By adjusting the KOH amount, GSPC-700-1:2 is prepared, which delivers the superior electrochemical performance. The specific capacitance of GSPC-700-1:2 is 345 F g^{-1} at 0.5 A g^{-1} and 280 F g^{-1} at 10 A g^{-1}. A symmetric supercapacitor device (SCD) fabricated from GSPC-700-1:2 exhibits a specific capacitance of 65 F g^{-1} at 0.5 A g^{-1}. After 10,000 charge and discharge cycles, SCD can maintain 83% capacitance retention at 5 A g^{-1}. Also, the power density of 301 W kg^{-1} is achieved at energy density of 13 W h kg^{-1}. These results indicate that GSPC-700-1:2 is an excellent

electrode material for supercapacitors.

Acknowledgements

This work was supported by the National Natural Science Foundation of China (Grant Nos. 21965007, 51671062 and 51871065), the Guangxi Natural Science Foundation (Grant No. 2018GXNSFFA281005), the Scientific Research and Technology Development Program of Guangxi (Grant Nos. AA19182014, AD17195073, AA17202030-1), Chinesisch-Deutsche Kooperationsgruppe (Grant No. GZ1528) and Guangxi Bagui Scholar Foundation, Guangxi Advanced Functional Materials Foundation and Application Talents Small Highlands.

References

[1] Zhang Y, Yuan X, Lu W, Yan Y, Zhu J, Chou T W. MnO_2 based sandwich structure electrode for supercapacitor with large voltage window and high mass loading. *Chemical Engineering Journal*. 2019; 368: 525-532.
[2] Zhang Y, He J, Gao Z, Li X. Converting eggs to flexible all-solid supercapacitors. *Nano Energy*. 2019; 65: 104045.
[3] Zhang W, Zou Y, Yu C, Zhong W. Nitrogen-enriched compact biochar-based electrode materials for supercapacitors with ultrahigh volumetric performance. *Journal of Power Sources*. 2019; 439: 227067.
[4] Maleki A, Masita M, Zeynab E. Adsorbent materials based on a geopolymer paste for dye removal from aqueous solutions. *Arabian Journal of Chemistry*. 2020; 13: 3017.
[5] Zhang L, Song X, Xiao B, Tan L, Ma H, Wang X, Li B, Guo D, Chu D. Highly graphitized and N, O co-doped porous carbon derived from leaves of viburnum sargenti with outstanding electrochemical performance for effective supercapacitors. *Colloids and Surfaces A: Physicochemical and Engineering Aspects*. 2019; 580(5): 123721.
[6] Yang N, Lin X Q, Lu Q F, Jin Y Q, Yang H. Polyaniline-modified renewable biocarbon composites as an efficient hybrid electrode for supercapacitors. *Ionics*. 2019; 25(3): 5459-5472.
[7] Maleki A, Hajizadeh Z Sharifi, V. A green, porous and eco-friendly magnetic geopolymer adsorbent for heavy metals removal from aqueous solutions. *Journal of Cleaner Production*. 2019; 215: 1233-1245.
[8] Wan L, Li X, Li N, Xie M, Du C, Zhang Y, Chen J. Multi-heteroatom-doped hierarchical porous carbon derived from chestnut shell with superior performance in supercapacitors. *Journal of Alloys and Compounds*. 2019; 790: 760-771.
[9] Serafin J, Baca M, Biegun M, Mijowska E, Kalenczuk R J, Nazzar J Srenscek, Michalkiewicz B. Direct conversion of biomass to nanoporous activated biocarbons for high CO_2 adsorption and supercapacitor applications. *Applied Surface Science*. 2019; 497(15): 143722.
[10] Emdadi Z, Asim N, Amin M, Ambar Yarmo M, Maleki A, Azizi M, Sopian K. Development of green geopolymer using agricultural and industrial waste materials with high water absorbency. *Applied Sciences*. 2017; 7: 514.
[11] Ragupathi V, Panigrahi P, Ganapathi Subramaniam N. g-C_3N_4 doped MnS as high-performance electrode material for supercapacitor application. *Materials Letters*. 2019; 246: 88-91.
[12] Ping Y, Liu Z, Li J, Han J, Yang Y, Xiong B, Fang P, He C. Boosting the performance of supercapacitors based hierarchically porous carbon from natural juncus effuses by incorporation of MnO_2. *Journal of Alloys and Compounds*. 2019; 805: 822-830.
[13] Phiri J, Dou J, Vuorinen T, Gane P A C, Maloney T C. Highly porous willow wood-derived activated carbon for high-performance supercapacitor electrodes. *ACS Omega*. 2019; 4(19): 18108-18117.
[14] Niu L, Shen C, Yan L, Zhang J, Lin Y, Gong Y, Li C, Sun C Q, Xu S. Waste bones derived nitrogen-doped carbon with high micropore ratio towards supercapacitor applications. *Journal of Colloid and Interface Science*. 2019; 547: 92-101.
[15] Shao C, Qiu S, Chu H, Zou Y, Xiang C, Xu F, Sun L. Nitrogen-doped porous microsphere carbons derived from glucose and aminourea for high-performance supercapacitors. *Catalysis Today*. 2018; 318: 150-156.
[16] Maleki A, Hajizadeh. Eco-friendly functionalization of magnetic halloysite nanotube with SO_3H for synthesis of dihydropyrimidinones. *Microporous and Mesoporous Materials*. 2018; 259: 46.
[17] Li H, Yuan D, Tang C, Wang S, Sun J, Li Z, Tang T, Wang F, Gong H, He C. Lignin-derived interconnected hierarchical porous carbon monolith with large areal / volumetric capacitances for supercapacitor. *Carbon*. 2016; 100: 151-157.

[18] Li P, Xie H, Liu Y, Wang J, Xie Y, Hu W, Xie T, Wang Y, Zhang Y. Molten salt and air induced nitrogen-containing graphitic hierarchical porous biocarbon nanosheets derived from kitchen waste hydrolysis residue for energy storage. *Journal of Power Sources*. 2019; 439: 227096.
[19] Li J, Wang J, Han K, Qi J, Li M, Teng Z, Wang M. Preparation of ginger straw based porous carbon using one-step pyrolysis process as electrode material for supercapacitor. *International Journal of Electrochemical Science*. 2019; 14: 10289-10305.
[20] Guardia L, Suarez L, Querejeta N, Madrera R Rodriguez, Suarez B, Centeno T A. Apple waste: A sustainable source of carbon materials and valuable compounds. *ACS Sustainable Chemistry and Engineering*. 2019; 7(20): 17335-17343.
[21] Maleki A, Hajizadeh Z. Magnetic aluminosilicate nanoclay: A natural and efficient nanocatalyst for the green synthesis of 4H-Pyran derivatives. *Silicon*. 2019; 11: 2789.
[22] Khodary S, Abomohra A, Enany G, Aboalhassan, Ng D, Wang S, Lian J. Sonochemical assisted fabrication of 3D hierarchical porous carbon for high-performance symmetric supercapacitor. *Ultrasonics Sonochemistry*. 2019; 58: 104617.
[23] Qu S, Wan J, Dai C, Jin T, Ma F. Promising as high-performance supercapacitor electrode materials porous carbons derived from biological lotus leaf. *Journal of Alloys and Compounds*. 2018; 751: 107-116.
[24] Chaturvedi V, Usangonvkar S, Shelke M V. Synthesis of high surface area porous carbon from anaerobic digestate and it's electrochemical study as an electrode material for ultracapacitors. *RSC Advances*. 2019; 9(62): 36343-36350.
[25] Bo X, Xiang K, Zhang Y, Shen Y, Chen S, Wang Y, Xie M, Guo X. Microwave-assisted conversion of biomass wastes to pseudocapacitive mesoporous carbon for high-performance supercapacitor. *Journal of Energy Chemistry*. 2019; 39: 1-7.
[26] Hajizadeh Z, Valadi K, Taheri-Ledari R, Maleki A. Convenient Cr (VI) removal from aqueous samples: executed by a promising clay-based catalytic system, magnetized by Fe_3O_4 nanoparticles and functionalized with humic acid. *ChemistrySelect*. 2020; 5: 2441-2448.
[27] Zhang W, Xu J, Hou D, Yin J, Liu D, He Y, Lin H. Hierarchical porous carbon prepared from biomass through a facile method for supercapacitor applications. *Journal of Colloid and Interface Science*. 2018; 530: 338-344.
[28] Raza W, Ali F, Raza N, Luo Y, Kim K H, Yang J, Kumar S, Mehmood A, Kwon E E. Recent advancements in supercapacitor technology. *Nano Energy*. 2018; 52: 441-473.
[29] Wang Y, Zhang M, Dai Y, Wang H Q, Zhang H, Wang Q, Hou W, Yan H, Li W, Zheng J C. Nitrogen and phosphorus co-doped silkworm-cocoon-based self-activated porous carbon for high performance supercapacitors. *Journal of Power Sources*. 2019; 438: 227045.
[30] Li Y, Wang X, Cao M. Three-dimensional porous carbon frameworks derived from mangosteen peel waste as promising materials for CO_2 capture and supercapacitors. *Journal of CO_2 Utilization*. 2018; 27: 204-216.
[31] Chu H, Shao C, Qiu S, Zou Y, Xiang C, Xu F, Sun L. Nitrogen-rich sandwich-like carbon nanosheets as anodes with superior lithium storage properties. *Inorganic Chemistry Frontiers*. 2018; 5(1): 225-232.
[32] Li H, Yuan D, Tang C, Wang S, Sun J, Li Z, Tang T, Wang F, Gong H, He C. Lignin-derived interconnected hierarchical porous carbon monolith with large areal/volumetric capacitances for supercapacitor. *Carbon*. 2016; 100: 151-157.
[33] Wu G, Shao C, Qiu S, Chu H, Zou Y, Xiang C, Zhang H, Xu F, Sun L. Guanine-derived nitrogen-doped ordered mesoporous carbons for lithium-ion battery anodes. *ChemistrySelect*. 2017; 2(31): 10076-10081.
[34] Maleki A. Green oxidation protocol: Selective conversions of alcohols and alkenes to aldehydes, ketones and epoxides by using a new multiwall carbon nanotube-based hybrid nanocatalyst via ultrasound irradiation. *Ultrasonics Sonochemistry*. 2018; 40: 460.
[35] Muzaffar A, Ahamed M B, Deshmukh K, Thirumalai J. A review on recent advances in hybrid supercapacitors: Design, fabrication and applications. *Renewable and Sustainable Energy Reviews*. 2019; 101: 123-145.
[36] Maleki A, Kari T, Aghaei M. Fe_3O_4@SiO_2@TiO_2-OSO_3H: an efficient hierarchical nanocatalyst for the organic quinazolines syntheses. *Journal of Porous Materials*. 2017; 24: 1481-1496.
[37] Liu S, Zhao Y, Zhang B, Xia H, Zhou J, Xie W, Li H. Nano-micro carbon spheres anchored on porous carbon derived from dual-biomass as high rate performance supercapacitor electrodes. *Journal of Power Sources*. 2018; 381: 116-126.
[38] Wang H, Sun X, Liu Z, Lei Z. Creation of nanopores on graphene planes with MgO template for preparing high-performance supercapacitor electrodes. *Nanoscale*. 2014; 6(12): 6577-6584.
[39] Xu G, Han J, Ding B, Nie P, Pan J, Dou H, Li H, Zhang X. Biomass-derived porous carbon materials with sulfur

and nitrogen dual-doping for energy storage. *Green Chemistry*. 2015; 17(3): 1668-1674.
[40] Zhang W, Xu J, Hou D, Yin J, Liu D, He Y, Lin H. Hierarchical porous carbon prepared from biomass through a facile method for supercapacitor applications. *Journal of Colloid and Interface Science*. 2018; 530: 338-344.
[41] Li Y, Wang G, Wei T, Fan Z, Yan P. Nitrogen and sulfur co-doped porous carbon nanosheets derived from willow catkin for supercapacitors. *Nano Energy*. 2016; 19: 165-175.
[42] Gong C, Wang X, Ma D, Chen H, Zhang S, Liao Z. Microporous carbon from a biological waste-stiff silkworm for capacitive energy storage. *Electrochimica Acta*. 2016; 220: 331-339.
[43] Zhu Y, Fang T, Hua J, Qiu S, Chu H, Zou Y, Xiang C, Huang P, Zhang K, Lin X, Yan E, Zhang H, Xu F, Sun L, Zeng J-L. Biomass-derived porous carbon prepared from egg white for high-performance supercapacitor electrode materials. *ChemistrySelect*. 2019; 4(24): 7358-7365.
[44] Li Z X, Zhang X, Liu Y C, Zou K Y, Yue M L. Controlling the BET surface area of porous carbon by using the Cd/C ratio of a Cd-MOF precursor and enhancing the capacitance by activation with KOH. *Chemistry-A European Journal*. 2016; 22(49): 17734-17747.
[45] Lei S, Chen L, Zhou W, Deng P, Liu Y, Fei L, Lu W, Xiao Y, Cheng B. Tetra-heteroatom self-doped carbon nanosheets derived from silkworm excrement for high-performance supercapacitors. *Journal of Power Sources*. 2018; 379: 74-83.
[46] Maleki A, Tooraj K. Novel Leaking-Free, Green, Double core/shell, palladium-loaded magnetic heterogeneous nanocatalyst for selective aerobic oxidation. *Catalysis Letters*. 2018; 148: 2929.
[47] Shao C, Wang Z, Wang E, Qiu S, Chu H, Zou Y, Xiang C, Xu F, Sun L. Self-assembly synthesis of nitrogen-doped mesoporous carbons used as high-performance electrode materials in lithium-ion batteries and supercapacitors. *New Journal of Chemistry*. 2017; 41(21): 12901-12909.
[48] Liu J, Deng Y, Li X, Wang L. Promising nitrogen-rich porous carbons derived from one-step calcium chloride activation of biomass-based waste for high performance supercapacitors. *ACS Sustainable Chemistry and Engineering*. 2015; 4(1): 177-187.
[49] Cheng P, Gao S, Zang P, Yang X, Bai Y, Xu H, Liu Z, Lei Z. Hierarchically porous carbon by activation of shiitake mushroom for capacitive energy storage. *Carbon*. 2015; 93: 315-324.
[50] Guo N, Luo W, Guo R, Qiu D, Guo J. Interconnected and hierarchical porous carbon derived from soybean root for ultrahigh rate supercapacitors. *Journal of Alloys and Compounds*. 2020; 834: 155115.
[51] Zhang Q, Huang Y, Xia D, L Hu, Li P, Tan L, Wang Y, He C, Shu D, Xie X. High-performance water desalination of heteroatom nitrogen- and sulfur co-doped open hollow tubular porous carbon electrodes via capacitive deionization. *Environmental Science: Nano*. 2019; 6: 3359-3373.